

# The polarity and dynamics of microtubule assembly in the budding yeast *Saccharomyces cerevisiae*

Paul S. Maddox\* †, Kerry S. Bloom\* and E.D. Salmon\*

\*Department of Biology, CB3280, University of North Carolina, Chapel Hill, North Carolina 27599-3280, USA

†e-mail: pmaddox@email.unc.edu

focus on  
CYTOSKELETON

**Microtubule assembly in *Saccharomyces cerevisiae* is initiated from sites within spindle pole bodies (SPBs) in the nuclear envelope. Microtubule plus ends are thought to be organized distal to the SPBs, while minus ends are proximal. Several hypotheses for the function of microtubule motor proteins in force generation and regulation of microtubule assembly propose that assembly and disassembly occur at minus ends as well as at plus ends. Here we analyse microtubule assembly relative to the SPBs in haploid yeast cells expressing green fluorescent protein fused to  $\alpha$ -tubulin, a microtubule subunit. Throughout the cell cycle, analysis of fluorescent speckle marks on cytoplasmic astral microtubules reveals that there is no detectable assembly or disassembly at minus ends. After laser-photobleaching, metaphase spindles recover about 63% of the bleached fluorescence, with a half-life of about 1 minute. After anaphase onset, photobleached marks in the interpolar spindle are persistent and do not move relative to the SPBs. In late anaphase, the elongated spindles disassemble at the microtubule plus ends. These results show for astral and anaphase interpolar spindle microtubules, and possibly for metaphase spindle microtubules, that microtubule assembly and disassembly occur at plus, and not minus, ends.**

The budding yeast *Saccharomyces cerevisiae* is an excellent model system for analysis of fundamental issues about coupling microtubule-assembly dynamics to force generation during polarized nuclear movements, chromosome segregation and the elongation of anaphase spindles<sup>1,2</sup>. In the G1 phase of the cell cycle, the cytoplasmic surface of a single SPB in the nuclear envelope nucleates three to five astral microtubules which randomly probe unknown sites at the cell cortex by dynamic instability; they grow out toward the cell cortex and shorten back to the SPB<sup>3,4</sup>. When the cell enters S phase, the SPB is duplicated, and the two SPBs subsequently separate, forming the mitotic spindle within the 1.5–2- $\mu$ m-diameter nucleus. The haploid spindle consists of about 8 overlapping interpolar microtubules (4 from each SPB) and 32 kinetochore microtubules (16 from each SPB), emanating from the inner surfaces of opposite SPBs<sup>5</sup>. Before anaphase, the nucleus moves to the neck between the mother and budding daughter cell, and the spindle becomes aligned along the mother–bud axis by means of pushing and pulling forces produced by interactions of cytoplasmic astral microtubules with the cortex<sup>4,6,7</sup>. Chromosomes oscillate back and forth between the spindle poles before anaphase, and are quickly segregated to their poles during anaphase A<sup>8</sup>. Spindle elongation into the bud (during anaphase B) involves both growth and sliding apart of overlapping interpolar microtubules, as well as pulling forces from astral microtubules<sup>9,10</sup>.

An important issue in understanding the coupling of assembly dynamics to force generation is whether assembly dynamics occur at SPBs or are solely a property of the plus ends. It has been proposed, in particular, that minus-end disassembly at SPBs shortens and pulls on astral and spindle microtubules, while minus-end assembly could generate pushing forces<sup>11</sup>. There is compelling evidence in support of this hypothesis. Of the six microtubule-associated motor proteins in yeast, two kinesin-related motors, Cin8 and Kip1, concentrate in the central spindle and push the overlapping interpolar microtubules apart<sup>9</sup> (reviewed in ref. 1). The other four microtubule motor proteins, the kinesin-related motors Kar3, Kip2, Kip3 and cytoplasmic dynein, localize in part to the SPBs. Mutations in these motor proteins lead to shorter or longer astral microtubule lengths *in vivo*, resulting in defects in spindle orienta-

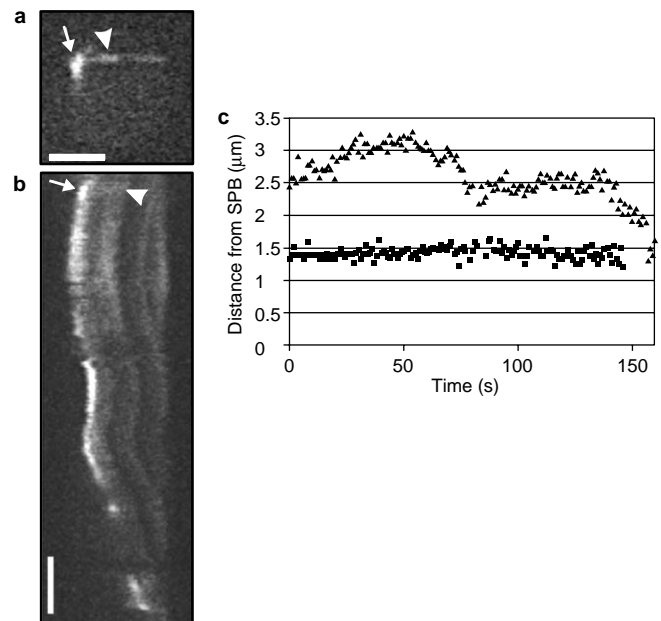


**Figure 1** FSM of an astral microtubule during the G1/S phase of the cell cycle. **a**, A single image of a G1/S-phase cell expressing GFP-tubulin, taken from a time-lapse experiment. The large arrowhead marks a bright fluorescent speckle, and the arrow marks the SPB. **b**, A kymograph (see Methods) of the microtubule shown in **a**. The kymograph shows that the distance between the SPB (arrow) and the tip of the microtubule at the cell cortex elongates and shortens over time, whereas the distance from the centre of the fluorescent speckle (large arrowhead) to the SPB remains constant. These distances are plotted in **c**. Squares indicate the distance from the SPB to the speckle, and triangles indicate the distance from the SPB to the tip of the microtubule, plotted against time. Scale bar in **a** represents 2  $\mu$ m, and in **b** represents 20 s. Note that the apparent changes in width of the indicated speckle region (arrowhead) over time are caused by loss of contrast resulting from photobleaching and fluctuations in focus.

tion (reviewed in ref. 2). Kar3 preferentially induces minus-end disassembly in *in vitro* motility assays<sup>12</sup>, and mutations in Kar3 lead to longer astral microtubules *in vivo*<sup>13,14</sup>. Kip3 and cytoplasmic dynein mutants also lead to longer than normal astral microtubules, while astral microtubules in Kip2 mutant cells are shorter<sup>6,14</sup>. As a result, it has been proposed that these motor proteins regulate or even drive polymer dynamics at microtubule minus ends located at the SPB<sup>11</sup>. This hypothesis is strengthened by observations in higher eukaryotic cells that have shown that spindle microtubules exhibit poleward movement (flux) coupled to minus-end disassembly at their poles (reviewed in ref. 15).

Here we use haploid yeast cells expressing  $\alpha$ -tubulin (*TUB1*) fused to green fluorescent protein (GFP) to test, in two ways, the possibility that microtubules in budding yeast exhibit dynamics at their minus ends. One technique used is fluorescent speckle microscopy (FSM), by which we analyse movements of fluorescent speckle marks on astral and anaphase spindle microtubules relative to the SPB. The second method is analysis of fluorescence redistribution after photobleaching (FRAP) in the mitotic spindle by laser microbeam irradiation.

## Results

### Cytoplasmic astral microtubules show no minus-end dynamics.

Figure 1a shows an example of a fluorescent speckled cytoplasmic astral microtubule in a G1/S-phase cell in strain 9dgt1 (see Methods). Microtubules acquire fluorescent speckles, or fluorescence discontinuities along the lattice, by random incorporation of a low concentration of fluorescent tubulin dimers along with unlabelled dimers<sup>16</sup>. Time-lapse FSM at 1 frame per second showed that, during growth and subsequent shortening of the astral microtubule, the indicated fluorescent speckle remained  $\sim 1.45\mu\text{m}$  from the SPB in the cell shown (Fig. 1b, c). To quantify possible speckle movements relative to the SPB, we drew least-squares best-fit lines through graphs plotting the distance between the SPB and the

speckle. We analysed only those cells in which an astral microtubule remained within the plane of focus during a nearly complete cycle of growth and shortening. Analysis of fluorescent speckles on ten microtubules in ten different cells revealed an average slope of  $-0.065\mu\text{m min}^{-1}$  (range  $-0.3$  to  $0.408\mu\text{m min}^{-1}$ ) over a total time of 20 min. Root-mean-square (r.m.s.) analysis showed that the average fluctuation of the measured data about the best-fit lines was  $0.173\mu\text{m}$  (range  $0.066$ – $0.469\mu\text{m}$ ; Table 1). These fluctuations could be due to assembly/disassembly at the SPB. However, as the average fluctuation is less than the  $0.25\text{-}\mu\text{m}$  theoretical resolution limit of the light microscope (for 514-nm light; ref. 17), they are most likely due to errors in measurement and/or slight focal shifts.

We also analysed cytoplasmic astral microtubules of mitotic cells by time-lapse FSM. Figure 2 shows a fluorescent speckle (Fig. 2a, arrowhead) on an astral microtubule extending from one SPB (Fig. 2a, arrow) of an anaphase spindle. The microtubule grew but

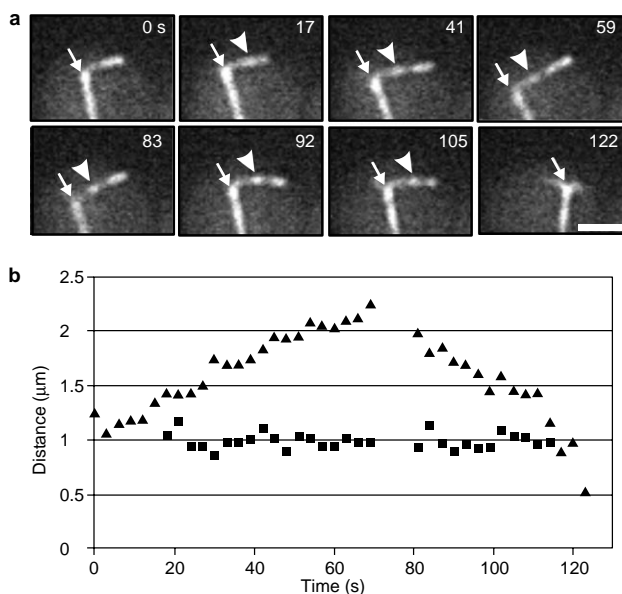


**Figure 2** **FSM of an astral microtubule during anaphase.** **a**, Selected frames from time-lapse observation of an anaphase cell expressing GFP-tubulin. The arrow marks the SPB and the arrowhead marks a speckle in the dynamic astral microtubule; the tip of the microtubule is in contact with the cortex to the right. The microtubule elongates (time points 41 s to 59 s) and then shortens (time points 59 s to 122 s) while the speckle remains a constant distance from the SPB. **b**, Microtubule growth and shortening (triangles) are plotted against time, as is the distance between the indicated speckle and SPB (squares). Scale bar represents  $2\mu\text{m}$ .

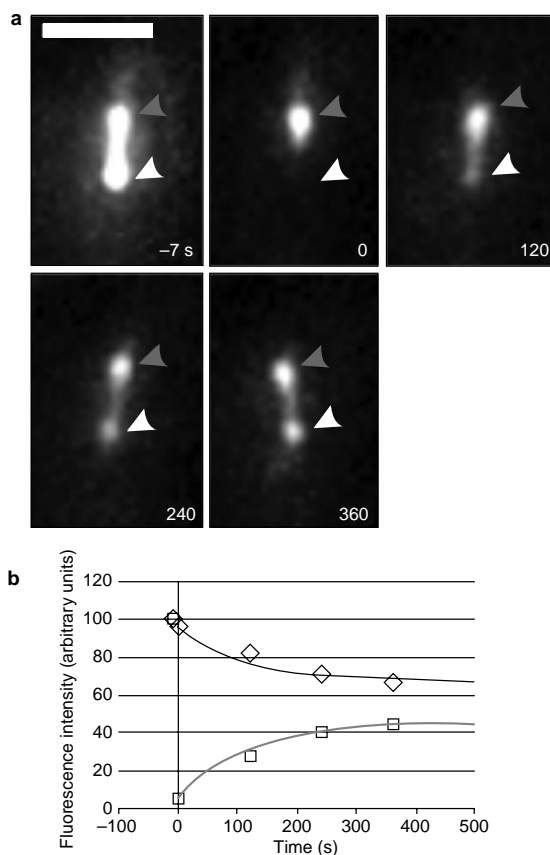


**Figure 3** **Partial fluorescence recovery after laser photobleaching of the metaphase spindle.** **a**, A metaphase spindle in a cell expressing GFP-tubulin that was photobleached in the lower half-spindle and then observed by time-lapse microscopy. The  $-7\text{s}$  time point shows the spindle before photobleaching. The laser was targeted to the lower half of the spindle (white arrowhead), which was exposed to the laser for 25 ms. Time point 0 shows that the upper half-spindle is still fluorescent (grey arrowhead) while the lower half has been bleached. Time-lapse analysis for 20 min revealed that the bleached portion of the spindle recovered fluorescence (white arrowhead), while the unbleached portion lost intensity, because of photobleaching by fluorescent exposures for image acquisition and incorporation of bleached tubulin subunits. Time points are given in seconds. **b**, The graph shows integrated intensity measurements of a  $5\text{ pixel}\times 5\text{ pixel}$  square placed over the bleached region (squares) and the unbleached region (diamonds) over time. These values are corrected for photobleaching that occurred during time-lapse image acquisition; a decrease from the initial value of  $\sim 20\%$  had occurred by the 360-s time point. Also plotted are the predicted rates of FRAP for bleached (grey line) and unbleached (black line) half-spindles. These theoretical values were derived using the first-order rate constant  $k$ , calculated as described in Methods. Scale bar in **a** represents  $2\mu\text{m}$ .

the fluorescent speckle did not move relative to the SPB (Fig. 2a, time point 5 s). The SPB moved closer to the cortex as the microtubule switched to shortening (Fig. 2a, 122 s). However, the fluorescent speckle maintained a distance of about 1  $\mu\text{m}$  from the SPB. The distances between speckles on eight cytoplasmic astral microtubules taken from seven mitotic cells (spindle length ranging from 1.5  $\mu\text{m}$  to 10  $\mu\text{m}$ ) to their respective SPBs were analysed by drawing best-fit lines as described above. The average slope of best-fit lines was 0.0007  $\mu\text{m min}^{-1}$  (range  $-0.138$  to 0.108  $\mu\text{m min}^{-1}$ ) and the average fluctuation was 0.134  $\mu\text{m}$  (r.m.s. analysis as above; Table 1). Therefore, cytoplasmic astral microtubules of mitotic cells, like those of G1/S cells, grow and shorten at their plus ends without changing length at their minus ends. We also observed several examples<sup>5</sup> (Fig. 2) in which plus-end growth and shortening at the cortex were coupled to movement of the SPB.

**Metaphase spindles are predominantly dynamic.** To determine whether microtubules within metaphase spindles are dynamic, we used laser photobleaching to selectively bleach one half of a 1.5–2- $\mu\text{m}$ -long spindle in strain 9dgt1. Cells containing metaphase spindles were photobleached using a diffraction-limited spot from the 488-nm line of an argon-ion laser and then recorded by time-lapse microscopy, initially at 30-s intervals and then at 2-min intervals. Figure 3a shows the results of one such experiment. Time point  $-7$  s shows the prebleached spindle. A 25-ms laser exposure targeted to the lower SPB (white arrowhead) effectively bleached the lower half of the spindle ( $\sim 95\%$  bleaching, 0 s) while having little immediate effect on the upper half of the spindle (5% loss in fluorescence intensity; grey arrowhead). Integrated intensity measurements of a 5 pixel $\times$ 5 pixel square placed over bleached or unbleached half-spindle regions are plotted versus time in Fig. 3b. The bleached region of this spindle recovered fluorescence with a time to half-maximal recovery of 56 s; the average for six spindles was  $52 \pm 23$  s, corresponding to an average first-order exponential rate constant of 0.0156 (Fig. 3a, b, 120 s; Table 2; see Methods). Fluorescence recovery was uniform relative to the initial intensity profile of the unbleached spindle. The unbleached half of the spindle lost fluorescence more quickly than did control spindles (as determined by measurements of control unbleached spindles; data not shown). The rate constant determined from the exponential recovery of fluorescence in the bleached half-spindle gave a good fit to the decay in fluorescence in the unbleached half-spindle (Fig. 3b; grey line, predicted recovery after bleaching; black line, predicted intensity loss from unbleached half-spindle), after correction for photobleaching produced by time-lapse image acquisition. Therefore, the observed loss of fluorescence in the unbleached half-spindle reflects incorporation of bleached tubulin subunits lost from the bleached half-spindle during steady-state turnover of the spindle microtubules. These data indicate that the photobleached GFP-tubulin subunits were able to re-incorporate into the microtubule lattice. In addition, the rate of fluorescence loss and recovery was the same in unirradiated and irradiated half-spindles, indicating that the microtubule dynamics were similar in bleached and unbleached

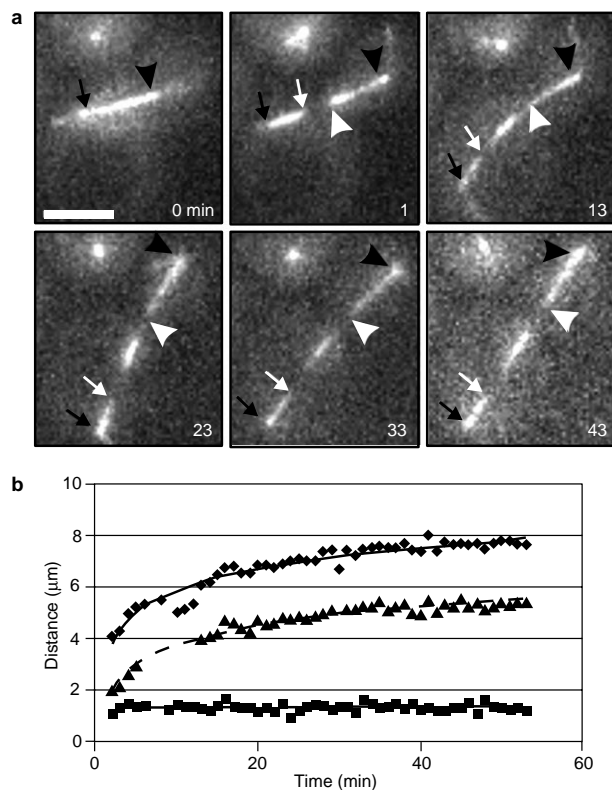


**Figure 4 Time-lapse observation of an anaphase spindle after laser photobleaching.** **a**, The time point 0 min shows a GFP-tubulin-expressing cell at the 4- $\mu\text{m}$  stage of anaphase spindle elongation. The laser was targeted midway between the SPBs (indicated by the black arrow and arrowhead), to the overlapping microtubules; time point 1 min shows the same spindle after laser exposure of 25-ms duration. The left and right margins of the bleach are marked by the white arrow and arrowhead, respectively. After 13 min, the photobleached mark has split into two marks as the overlapping microtubules slid past each other while the spindle continued to elongate. **b**, The distance between the two SPBs (diamonds), the distance between the left margin of the original mark and the lower SPB (white arrow to black arrow, squares) and the distance from the right margin of the original mark to the lower SPB (white arrowhead to black arrow, triangles) are plotted against time. Scale bar in **a** represents 4  $\mu\text{m}$ .

regions. The corrected ratio of FRAP between bleached and unbleached regions after full recovery was about 63% (Table 2). This indicates that the bleached region contained a stable component (about 37%) that did not recover fluorescence. For metaphase spindles that were laser-irradiated just before the onset of anaphase, the

**Table 1 Statistical analysis of FSM and FRAP marks relative to SPBs**

Technique	Slope ( $\mu\text{m min}^{-1}$ )*	Fluctuation (r.m.s.) ( $\mu\text{m}$ )†	Total time (min)‡	Number of samples§
FSM of astral microtubules:				
G1/S phase	$-0.065 \pm 0.229$	0.173	20	10
M phase	$0.0007 \pm 0.229$	0.134	13	8
Photobleached marks on anaphase spindles	$0.0057 \pm 0.011$	0.156	109	9
FSM of spindle disassembly	$0.009 \pm 0.038$	0.123	12	4

\* The slope is determined from the equation of a least-squares best-fit line drawn through data showing the distance between a fluorescent mark and the SPB, plotted against time (see Methods). The value shown is the average taken from the number of samples indicated.

† r.m.s. (root mean square) was calculated about the least-squares best-fit line through data showing the distance between a fluorescent mark and the SPB, plotted against time (see Methods). The value shown is an average taken from the number of samples indicated.

‡ Total duration of all samples measured for a given parameter.

§ Number of microtubules measured.

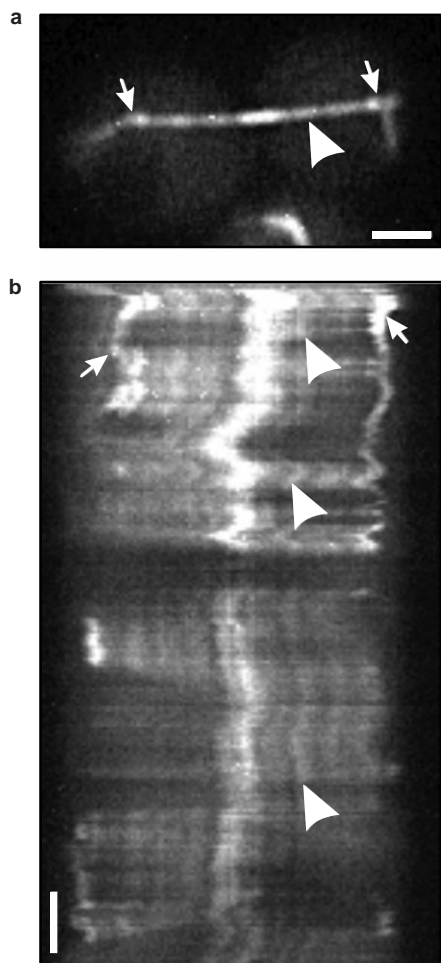


**Figure 5 FSM of a late-anaphase spindle.** **a**, A GFP-tubulin-expressing cell in late anaphase. Arrows mark the SPBs, and the arrowhead marks a selected fluorescent speckle. The entire spindle oscillates left and right; however, the kymograph in **b** shows that the speckles, exemplified by the indicated speckle (arrowhead), do not move relative to the SPBs. Dark areas in the kymograph are caused by focal shifts during the time-lapse experiment. The bright region in the middle of the spindle is the site of overlap of the 2–4 spindle microtubules from either pole<sup>5</sup>. Scale bar in **a** represents 2 $\mu$ m, and in **b** represents 20 s.

unrecovered bleach mark was visible on the inter-polar microtubules throughout spindle elongation in anaphase B (data not shown). Laser exposure in metaphase did not damage the spindle, as microbeam-irradiated cells proceeded through anaphase and cell division with normal kinetics (anaphase rates: fast phase, 0.65 $\mu$ m min<sup>-1</sup>,  $n=4$ ; slow phase, 0.3 $\mu$ m min<sup>-1</sup>,  $n=4$ ; refs 9, 18).

**Spindle microtubules elongate at their plus ends in anaphase B.**

Spindle microtubules were laser-photobleached during various stages of anaphase-B spindle elongation (spindle length 2–10 $\mu$ m at time of bleach) to allow us to observe inter-polar microtubule dynamics. Time-lapse sequences showed that the central spindle microtubules did not recover fluorescence after photobleaching. Figure 4 shows one experiment in which an anaphase spindle was bleached when it was 4  $\mu$ m in length (time point 0 min). The black arrow and arrowhead mark the SPBs and the white arrow and arrowhead indicate the margins of the bleach mark. Anaphase proceeded with normal elongation kinetics (refs 9, 18), indicating that laser exposure was not detrimental to the mechanism of spindle elongation and did not sever the spindle. Instead, the photobleached mark split into two marks as the spindle continued to elongate. Splitting of the mark would be expected as a

**Table 2 Measured parameters of FRAP in pre-anaphase spindles**

Sample number	First-order rate constant (k)*	t <sub>1/2</sub> (s)*	Recovery of bleached region†
1	0.0274	25.32	0.66
2	0.0176	39.384	0.68
3	0.0206	33.66	0.58
4	0.0124	55.92	0.59
5	0.0088	78.78	0.63
6	0.0087	79.8	0.66
Average	0.0159	52.144	0.63
Standard deviation	0.0074	23.292	0.038

\* Calculated as described in Methods.

† Ratio of bleached:unbleached region after recovery.

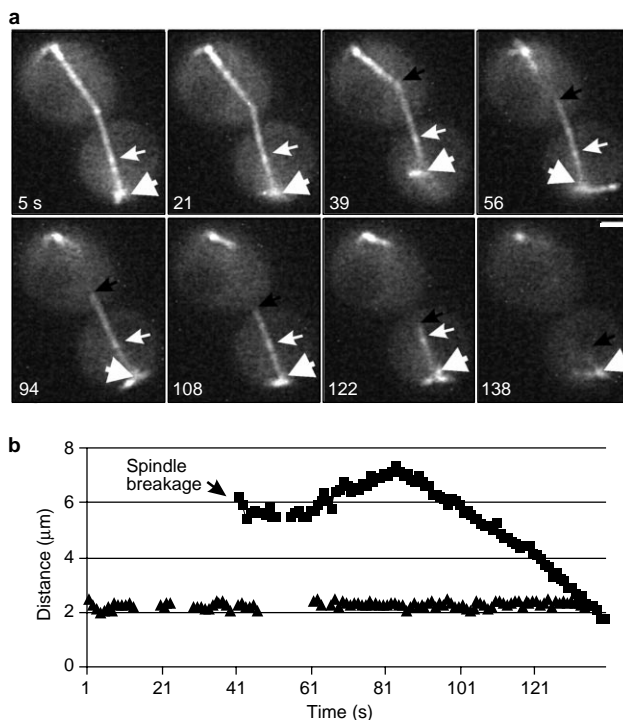


**Figure 6 FSM of spindle disassembly in telophase.** **a**, Time-lapse FSM of a telophase cell expressing GFP-tubulin. The large arrow marks the SPB and the small white arrow marks a fluorescent speckle in the spindle microtubules. The distance from the speckle to the SPB remains constant over time as the spindle kinks and then disassembles (black arrow). **b**, The distances between the SPB and the speckle (triangles), and between the SPB and the microtubule tip (squares), are plotted against time. The free end of the lower half-spindle elongated after losing contact with the upper half-spindle, as can be seen in the graph. Scale bar in **a** represents 2  $\mu$ m.

result of anaphase motor proteins (Cin8 and Kip1) sliding overlapping antiparallel spindle microtubules apart (refs 1, 9). Our data show that tubulin polymerized at the plus ends of the microtubules during elongation. Figure 4b shows a graph of the distance from the SPB proximal to the bleached region (Fig. 4a, black arrow; Fig. 4b,  $y=0$ ) to the margins of the bleach mark (Fig. 4a, white arrow; Fig. 4b, squares represent the proximal margin; Fig. 4a, white arrowhead; Fig. 4b, triangles represent the distal margin) and distal SPB (Fig. 4a, black arrowhead; Fig. 4b, diamonds). Statistical analysis of nine cells (total observation time 109 min) using best-fit lines (as described above and in Methods) revealed that the distance from the SPB to the mark did

not change over time (average slope  $0.006 \mu\text{m min}^{-1}$ ) and that fluctuations were less than the resolution limit of the microscope (average r.m.s.  $0.156 \mu\text{m}$ ), as was observed for fluorescent speckles on astral microtubules (Table 1).

Spindle microtubule dynamics could also be observed by FSM during later stages of anaphase (spindle length  $8\text{--}10 \mu\text{m}$ ). At this stage, the interpolar spindle contains about four or fewer interpolar microtubules<sup>5</sup>. In Fig. 5a, one frame from an FSM time-lapse sequence is shown. The arrows point to the SPBs and the arrowhead indicates a selected fluorescent speckle on the anaphase spindle. Fig. 5b shows a kymograph of the time lapse. The kymograph shows that the entire spindle moved relative to the mother–bud neck and along the mother–bud axis, as can be seen by lateral movements of the spindle and by dark spaces as the spindle transiently rotated out of focus. Despite spindle movements, fluorescent speckles did not move relative to the SPBs over the course of this experiment. Statistical analysis by best-fit line as described above resulted in an average fluorescent speckle to SPB velocity of  $0.0012 \mu\text{m min}^{-1}$  with fluctuations measured by r.m.s. of  $0.264 \mu\text{m}$  (Table 1).

The FSM images in Fig. 6 show that telophase spindles disassemble by plus-end depolymerization. Figure 6a shows a time-lapse sequence of a telophase spindle undergoing disassembly. The small white arrow points out a fluorescent speckle; the lower SPB is marked by the large white arrow; and, beginning at 39 s, the black arrow marks the end of the disassembling spindle. The telophase spindle kinked in the middle where the two overlapping halves of the interpolar spindle met (time points 5 and 21 s). At time point 39 s, the spindle kinked even more and separated at that point. The lower SPB was then drawn toward the bud neck as the half-spindle shortened. Then the lower half-spindle increased in length at its free plus end (Fig. 6b, squares). The end of the half-spindle shortened completely back to the SPB while the fluorescent speckle maintained its position  $\sim 2 \mu\text{m}$  from the SPB (Fig. 6a, small white arrow; Fig. 6b, triangles). Statistical analysis of best-fit lines through the plotted data showed that fluorescent speckles did not move toward the SPB during spindle disassembly (slope  $0.009 \mu\text{m min}^{-1}$ ; r.m.s.  $0.123 \mu\text{m}$ ;  $n = 4$  cells; Table 1).

## Discussion

Here we have used two methods of fluorescently marking the microtubule lattice to test whether or not microtubule minus-end assembly dynamics are involved in force generation during microtubule-mediated processes. We have studied astral microtubules at different stages of the cell cycle, spindle microtubules in metaphase, and interpolar spindle microtubules in anaphase.

Cytoplasmic astral microtubules are needed for the orientation and positioning of the nucleus during the mitotic cell cycle of budding yeast<sup>19</sup>. This subset of microtubules is thought to help in orientating the mitotic spindle by a combination of pushing and pulling forces exerted on the cell cortex, coupled with microtubule assembly and disassembly<sup>4,10</sup>. Our results show that minus ends contribute little or nothing to assembly dynamics during the lifetime of cytoplasmic astral microtubules. In addition, the growth of astral microtubule plus ends at the cell cortex can push the SPB away from the cortex, while shortening of the plus ends at cortical attachment sites can result in SPBs moving closer to the cortex (Fig. 2). These results are identical to those found in previous studies using FRAP and FSM to study astral microtubules during the mating process<sup>20</sup>. In mating cells, plus ends of the astral microtubule array form dynamic attachments to the cell cortex at the tip of the shmoo projection. These mating microtubule arrays produce force (in the form of nuclear oscillation towards and away from the shmoo tip) coupled to plus-end, and not minus-end, microtubule dynamics<sup>20</sup>. Thus the regulation of astral microtubule lengths and/or the coupling of pushing and pulling forces to astral microtubule assembly dynamics in both the vegetative cell cycle and during mating are a property of plus and not minus ends.

Kinetochores microtubules are necessary for chromosome segre-

gation during anaphase. The results of our metaphase FRAP experiments indicate that kinetochores microtubules are dynamic, because the percentage of recovered fluorescence (63%) correlates well with the fraction of kinetochores versus interpolar microtubules: of the 24 microtubules, 16 (66%) are kinetochores microtubules (the remaining 8 microtubules are overlapping interpolar microtubules<sup>5</sup>). In addition, the 53-s average half-life of fluorescence recovery measured in our experiments is predicted by the rate and extent of chromosome oscillations between the SPBs<sup>8</sup>. Therefore, the magnitude and rate of change in fluorescence intensity along the spindle after laser photobleaching (that is, partial recovery in the bleached region and partial loss in the unbleached region) could be due to the growth and shortening of kinetochores microtubules, coupled to oscillations of metaphase chromosomes.

The resolution in our FRAP experiments was not sufficient for us to be able to determine the polarity of microtubule dynamics during fluorescence recovery. However, a recent report<sup>21</sup> has shown, by electron microscopy, that all minus ends (cytoplasmic and nuclear) have the same tapered or capped structure. Likewise all detectable microtubule ends distal from the SPB (plus ends) are open or splayed<sup>21</sup>. As all nuclear microtubules have a capped structure identical to that of the inactive minus ends of cytoplasmic and anaphase spindle microtubules, it seems likely that the minus ends of kinetochores microtubules are also inactive. This comparison points to the plus end of the kinetochores microtubule as the site of assembly and disassembly required for chromosome movements. However, it is possible that the structural appearance of a microtubule end does not reflect its assembly dynamics, and that the dynamics of minus ends could change between metaphase and anaphase.

In anaphase in budding yeast, our results show that the elongation of interpolar spindles is coupled to microtubule growth at the overlapping plus ends, as has been shown for diatom central spindles<sup>22</sup>, the midbody in tissue cells<sup>23</sup>, and, more recently, for the interpolar anaphase spindle of the fission yeast *Schizosaccharomyces pombe*<sup>24</sup>. The kinesin Kip3 has been localized to the anaphase spindle midzone, and therefore could help regulate microtubule plus-end growth at this site<sup>14</sup>. Our results provide new information on interpolar spindle disassembly; it occurs at plus ends after the overlapping interpolar arrays separate in late anaphase.

Minus-end disassembly coupled to microtubule poleward movement (flux) was previously proposed to be a ubiquitous property of microtubules<sup>25</sup>. Flux has been observed in the microtubules of mitotic spindles of tissue culture cells and *Xenopus* egg extracts<sup>25–27</sup>. Poleward movement of microtubules has also been seen in lamellipodia of migrating tissue cells<sup>28</sup>. Our results show that microtubule flux does not occur in astral and interpolar spindle microtubules in yeast. One possible explanation for this unexpected result is that microtubules that are attached directly to the nucleating body (the SPB in yeast and the centrosome in higher organisms) have stable minus ends. In fact, the microtubules were not directly attached to the centrosome in those instances in which flux was observed<sup>26–28</sup>, and centrosomal microtubules in mitotic newt lung cells do not exhibit poleward flux<sup>29</sup>. If microtubules are unable to produce force by poleward flux when directly attached to nucleating centres, then regulation of minus-end release<sup>30</sup> might be important in maintaining the balance of forces during the lifetime of cells.

The question remains of how mutations in the motor proteins Kar3, Kip2, Kip3 and dynein give rise to phenotypes such as longer or shorter astral microtubules in yeast. On the basis of our results, it appears that such phenotypes do not result from regulation of the dynamics of microtubule assembly and disassembly at minus ends. □

## Methods

### Yeast strains and GFP constructs.

We used the haploid yeast strain 9d (*MAT $\alpha$* , *lys2-801*, *his3-200*, *ura3-52*, *leu2-3, 112*). To visualize dynamic microtubules *in vivo*, we transformed strain 9d with the integrating plasmid pAFS125 (a gift from A. Straight). The resulting strain, 9dgt1, contained GFP fused to the amino terminus of the major yeast  $\alpha$ -tubulin, Tub1. The complementary DNA encoding this fusion protein was integrated into the

URA3 gene and under the control of the native *TUB1* promoter.

### Culture preparation for microscopy.

Strain 9dgt1 was grown to mid-logarithmic phase in liquid media and then placed in a growth chamber for time-lapse multi-mode imaging. Briefly, gelatin (Sigma; catalogue number G-2500) was added to minimal synthetic medium to 25% (*w/v*) then heated to 65 °C for mixing of the gelatin and medium. For preparation of growth chambers (made fresh for each experiment), the gelatin/medium mixture was again heated to 65 °C to liquefy it; 50 µl were then placed between two cleaned microscope slides and pressure was applied until the gelatin had solidified. The slides were then pried apart, leaving a thin gelatin slab on one of the slides. 1 ml of the log-phase culture was spun in a microfuge for 10 s to produce a pellet, and then resuspended in 1 ml sterile water. This mixture was then repelleted and resuspended in 100 µl sterile water. 10 µl of the concentrated log-phase cells were then pipetted onto the gelatin slab and covered with an 18 mm × 18 mm number 1 coverglass. The chamber was then sealed with Valap (1:1:1 vaseline:lanolin:paraffin) and placed on the microscope for imaging. All imaging was done at 25 °C.

### FSM of GFP-tubulin in live cells.

The technique for achieving fluorescent speckle marks along dynamic polymers has been described in detail elsewhere<sup>16</sup>. The specific application of FSM to observation of microtubules in budding yeast has also been described<sup>20</sup>. A brief description of the imaging system follows. Cells prepared as described above were time-lapse imaged on a Nikon E600FN fixed-stage upright microscope using a 100×/1.4 NA Plan Apo bright-field objective, a 100-W mercury arc lamp (attenuated to ~10%) fluorescent-light source and a Chroma (Brattletown, VT) Hy-Q FITC filter set. Images were collected digitally as described<sup>20</sup>. Briefly, Metamorph software (Universal Imaging Corp., West Chester, PA) was used to control a Hamamatsu Photonics (Bridgewater, NJ) Orca c4742-95 chilled charge-coupled-device (CCD) camera, a Nikon *z*-axis stepping motor, and a Uniblitz shutter (Vincent Associates, Rochester, NY). Images were collected at various intervals depending on the experiment, ranging from 5 frames s<sup>-1</sup> to 1 frame per 10 s. Exposure times also varied with the experiment, and ranged from 100 ms to 800 ms. The CCD chip was operated at full resolution, not binned, to retain the maximum spatial resolution required to image fluorescent speckles along microtubules at ×100 total magnification to the camera. Single focal planes were collected at each time point instead of a through-focus *z*-series, to ensure that speckles were not produced by focal aberrations.

### Laser photobleaching of GFP-tubulin in live cells.

Photobleaching techniques have been well characterized<sup>21</sup>. A description of our present photobleaching instrument is below. Cells were prepared as described above and imaged on a Nikon TE300 inverted microscope using a 100×/1.4 NA Plan Apo bright-field objective, a 100-W mercury arc (attenuated to ~10%) fluorescent-light source, and a Chroma Hy-Q FITC filter set. The 488-nm line from an argon laser (Spectra-Physics, Mountain View, CA) was selected by a band-pass filter and then shuttered to control exposure. The laser was then passed through a beam expander (to maximize the size of the beam in the back aperture of the objective) and focused to a spot on the field diaphragm. Analysis of the focused beam showed that, when using the 100×/1.4 NA Plan Apo bright-field objective, the spot had a gaussian profile and a diameter at half-maximal intensity of 0.8 µm. Images were collected as described for FSM with the following changes: images were binned 2×2 to increase signal-over-camera noise fourfold, as maximum spatial resolution was not required here. Also, a through-focal *z*-series stack consisting of five frames acquired at 0.5-µm intervals was acquired at each time point. These procedures did not impair imaging of photobleached marks because they are distinct from the rest of the microtubules in the cell. A typical experiment consisted of imaging microtubules in a cell to target the laser beam to the proper structure, opening the laser shutter for 25 ms then recording the cell by time-lapse microscopy, taking a *z*-series every 30 s or 2 min, depending on the experiment. Post-processing of time-lapse sequences included constructing a single image by maximum-brightness projection of the *z*-series from each time point as described<sup>22</sup>. Images were processed and analysed using Metamorph software. Figures were constructed in CorelDraw (version 7.0).

### Statistical analysis of FSM and FRAP data.

Metamorph software was used to measure selected parameters (distance or fluorescence intensity) from time series that were suitable for analysis. For measurements of the movement of fluorescent speckles or photobleached marks relative to the SPB, images were calibrated using a stage micrometer and the distance between the stated regions was measured three times for each time point. The data were exported to Excel 97 (Microsoft); the three sets of data were averaged and the average distance over time was plotted by *X*-*Y* scatter. Best-fit lines were drawn through the data by the least-squares method and the slope was reported as a measure of net velocity over the given time period (Fig. 1c, Table 1). The r.m.s. was then calculated for the data to determine a measure of fluctuation about the average distance (Table 1).

Measurements of FRAP were made on a maximum-brightness projection of *z*-series for each time point from time-lapse sequences at 2-min intervals. A 5 pixel × 5 pixel square (corresponding to an area of 0.5 µm × 0.5 µm) was placed over the bleached half-spindle, unbleached half-spindle, or a cytoplasmic reference site (for subtracting background) and integrated intensity was measured three independent times for each set of data. The average was analysed as follows. After exporting from Metamorph to Excel 97, the data were corrected for background intensity and photobleaching that takes place during image acquisition (correction derived from an average value of six unirradiated cells observed under the same conditions as experimental at corresponding stages of the cell cycle) and then normalized to an arbitrary starting value of 1. The first-order rate constant *k* was determined as described<sup>23</sup>. Briefly, the exponential function  $F_{int} - F(t) = [F_{int} - F(0)] e^{-kt}$  (equation 1) describes fluorescence redistribution in the bleached half-spindle after laser irradiation, while  $F(t) - F_{int} = [F(0) - F_{int}] e^{-kt}$  (equation 2) describes fluorescence decay in the unbleached half-spindle. In these functions,  $F_{int}$  is the intensity of the bleached (equation 1) or unbleached (equation 2) region after maximal recovery;  $F(t)$  is the intensity of the measured region at *t*=0 (first time point after laser irradiation). The first-order rate constant *k* is derived from the slope of a best-fit line through graphs of  $\ln[F_{int} - F(t)]$  versus time for bleached regions, and  $\ln[F(t) - F_{int}]$  versus time for unbleached regions. The  $t_{1/2}$  of fluorescence redistribution is then calculated by  $t_{1/2} = \ln 2/k$  (equation 3). Figure 3b shows a plot of the derived data using the average *k* (from six experiments) applied to equations 1 and 2 along with the actual observed redistribution of tubulin fluorescence in bleached and unbleached regions of the spindle. Table 2 shows the rate constant.

Kymographs were produced in Metamorph software by using the 'kymograph' function. Briefly, a line (*x*-dimension) of width 5 pixels was drawn along the microtubule or spindle (*y*-dimension). This

line was then analysed by the software, and the brightest pixel in the *x*-dimension for each point along the line (*y*-dimension) was recorded. The finished image consists of the measurement described above performed for each time point, placed one after another to display intensity differences over time.

RECEIVED 27 AUGUST 1999; REVISED 11 OCTOBER 1999; ACCEPTED 19 NOVEMBER 1999; PUBLISHED 8 DECEMBER 1999.

- Hoyt, M. A. & Geiser, J. R. Genetic analysis of the mitotic spindle. *Annu. Rev. Genet.* **30**, 7–33 (1996).
- Saunders, W. S. Action at the ends of microtubules. *Curr. Opin. Cell Biol.* **11**, 129–133 (1999).
- Carminati, J. L. & Stearns, T. Microtubules orient the mitotic spindle in yeast through dynein-dependent interactions with the cell cortex. *J. Cell Biol.* **138**, 629–641 (1997).
- Shaw, S. L., Yeh, E., Maddox, P., Salmon, E. D. & Bloom, K. Astral microtubule dynamics in yeast: a microtubule-based searching mechanism for spindle orientation and nuclear migration into the bud. *J. Cell Biol.* **139**, 985–994 (1997).
- Winey, M. *et al.* Three-dimensional ultrastructural analysis of the *Saccharomyces cerevisiae* mitotic spindle. *J. Cell Biol.* **129**, 1601–1615 (1995).
- Cottingham, F. R. & Hoyt, M. A. Mitotic spindle positioning in *Saccharomyces cerevisiae* is accomplished by antagonistically acting microtubule motor proteins. *J. Cell Biol.* **138**, 1041–1053 (1997).
- Theesfeld, C. L., Irazoqui, J. E., Bloom, K. & Lew, D. J. The role of actin in spindle orientation changes during the *Saccharomyces cerevisiae* cell cycle. *J. Cell Biol.* **146**, 1019–1032 (1999).
- Straight, A. F., Marshall, W. F. & Murray, A. W. Mitosis in living budding yeast: anaphase A but no metaphase plate. *Science* **277**, 574–578 (1997).
- Straight, A. F., Sedat, J. W. & Murray, A. W. Time-lapse microscopy reveals unique roles for kinesins during anaphase in budding yeast. *J. Cell Biol.* **143**, 687–694 (1998).
- Lee, L., Klee, S. K., Evangelista, M., Boone, C. & Pellman, D. Control of mitotic spindle position by the *Saccharomyces cerevisiae* formin Bni1p. *J. Cell Biol.* **144**, 947–961 (1999).
- Huyett, A., Kahana, J., Silver, P., Zeng, X. & Saunders, W. S. The Kar3p and Kip2p motors function antagonistically at the spindle poles to influence cytoplasmic microtubule numbers. *J. Cell Sci.* **111**, 295–301 (1998).
- Endow, S. A. *et al.* Yeast Kar3 is a minus-end microtubule motor protein that destabilizes microtubules preferentially at the minus ends. *EMBO J.* **13**, 2708–2713 (1994).
- Meluh, P. B. & Rose, M. D. KAR3, a kinesin-related gene required for yeast nuclear fusion. *Cell* **60**, 1029–1041 (1990).
- Todd M. DeZwaan, T. M., Eric Ellingson, E., David Pellman, D. & Roof, D. M. Kinesin-related KIP3 of *Saccharomyces cerevisiae* is required for a distinct step in nuclear migration. *J. Cell Biol.* **138**, 1023–1040 (1997).
- Desai, A. & Mitchison, T. J. Microtubule polymerization dynamics. *Annu. Rev. Cell Dev. Biol.* **13**, 83–117 (1997).
- Waterman-Storer, C. M. & Salmon, E. D. How microtubules get fluorescent speckles. *Biophys. J.* **75**, 2059–2069 (1998).
- Salmon, E. D. *et al.* A high-resolution multimode digital microscope system. *Methods Cell Biol.* **56**, 185–215 (1998).
- Yeh, E., Skibbens, R. V., Cheng, J. W., Salmon, E. D. & Bloom, K. (1995). Spindle dynamics and cell cycle regulation of dynein in the budding yeast, *Saccharomyces cerevisiae*. *J. Cell Biol.* **130**, 687–700 (1995).
- Jacobs, C. W., Adams, A. E., Szaniszlo, P. J. & Pringle, J. R. Functions of microtubules in the *Saccharomyces cerevisiae* cell cycle. *J. Cell Biol.* **107**, 1409–1426 (1988).
- Maddox, P. *et al.* Microtubule dynamics from mating through the first zygotic division in the budding yeast *Saccharomyces cerevisiae*. *J. Cell Biol.* **144**, 977–987 (1999).
- O'Toole, E. T., Winey, M. & MacIntosh, J. R. High-voltage electron tomography of spindle pole bodies and early mitotic spindles in the yeast *Saccharomyces cerevisiae*. *Mol. Biol. Cell* **10**, 2017–2031 (1999).
- Wein, H., Foss, M., Brady, B. & Cande, W. Z. DSK1, a novel kinesin-related protein from the diatom *Cylindrotheca fusiformis* that is involved in anaphase spindle elongation. *J. Cell Biol.* **133**, 595–604 (1996).
- Saxton, W. M. & McIntosh, J. R. Interzone microtubule behavior in late anaphase and telophase spindles. *J. Cell Biol.* **105**, 875–886 (1987).
- Mallavarapu, A., Sawin, K. & Mitchison, T. A switch in microtubule dynamics at the onset of anaphase B in the mitotic spindle of *Schizosaccharomyces pombe*. *Curr. Biol.* **9**, 1423–1426 (1999).
- Sawin, K. E. & Mitchison, T. J. Microtubule flux in mitosis is independent of chromosomes, centrosomes, and antiparallel microtubules. *Mol. Biol. Cell* **5**, 217–226 (1994).
- Mitchison, T. J. Polewards microtubule flux in the mitotic spindle: evidence from photoactivation of fluorescence. *J. Cell Biol.* **109**, 637–652 (1989).
- Desai, A., Maddox, P. S., Mitchison, T. J. & Salmon, E. D. Anaphase A chromosome movement and poleward spindle microtubule flux occur at similar rates in *Xenopus* extract spindles. *J. Cell Biol.* **141**, 703–713 (1998).
- Waterman-Storer, C. M., Desai, A., Bulinski, J. C. & Salmon, E. D. Fluorescent speckle microscopy, a method to visualize the dynamics of protein assemblies in living cells. *Curr. Biol.* **8**, 1227–1230 (1998).
- Waterman-Storer, C. M. & Salmon, E. D. Actomyosin-based retrograde flow of microtubules in the lamella of migrating epithelial cells influences microtubule dynamic instability and turnover and is associated with microtubule breakage and treadmilling. *J. Cell Biol.* **139**, 417–434 (1997).
- Keating, T. J., Peloquin, J. G., Rodionov, V. L., Momcilovic, D. & Borisy, G. G. Microtubule release from the centrosome. *Proc. Natl Acad. Sci USA* **94**, 5078–5083 (1997).
- Salmon, E. D. & Wadsworth, P. in *Applications of Fluorescence in the Biomedical Sciences* (eds Taylor, D. L., Waggoner, A. S., Lanni, F., Murphy, R. F. & Birge, R. R.) 377–403 (Alan R. Liss, New York, 1986).
- Shaw, S. L., Yeh, E., Bloom, K. & Salmon, E. D. Imaging green fluorescent protein fusion proteins in *Saccharomyces cerevisiae*. *Curr. Biol.* **7**, 701–704 (1997).

### ACKNOWLEDGEMENTS

P.S.M. thanks members of the Salmon and Bloom laboratories for support and A. Straight for the gift of GFP-Tub1. We also thank Nikon, Hamamatsu Photonics and Universal Imaging for the loan of equipment used for development of our imaging systems. This work was supported by NIH grants GM32238 (to K.S.B.) and GM24364 (to E.D.S.).

Correspondence and requests for materials should be addressed to P.S.M.